Nanocrystal Growth

DOI: 10.1002/anie.201403530

Screw-Dislocation-Driven Bidirectional Spiral Growth of Bi_2Se_3 Nanoplates**

*Awei Zhuang, Jia-Jun Li, You-Cheng Wang, Xin Wen, Yue Lin, Bin Xiang, Xiaoping Wang, and Jie Zeng**

Abstract: *Bi_2Se_3 attracts intensive attention as a typical thermoelectric material and a promising topological insulator material. However, previously reported Bi_2Se_3 nanostructures are limited to nanoribbons and smooth nanoplates. Herein, we report the synthesis of spiral Bi_2Se_3 nanoplates and their screw-dislocation-driven (SDD) bidirectional growth process. Typical products showed a bipyramid-like shape with two sets of centrosymmetric helical fringes on the top and bottom faces. Other evidence for the unique structure and growth mode include herringbone contours, spiral arms, and hollow cores. Through the manipulation of kinetic factors, including the precursor concentration, the pH value, and the amount of reductant, we were able to tune the supersaturation in the regime of SDD to layer-by-layer growth. Nanoplates with preliminary dislocations were discovered in samples with an appropriate supersaturation value and employed for investigation of the SDD growth process.*

Screw dislocation, as a universal line defect, can act as a driving force to break the symmetry of crystal growth and promote the formation of anisotropic nanostructures.[1–3] Screw-dislocation-driven (SDD) growth was predicted by classical crystal-growth theory and distinguished from the other two basic growth modes, that is, layer-by-layer (LBL) growth and dendritic growth, in terms of the supersaturation conditions.[4] At very low supersaturations, only SDD growth is permitted, since there are step edges to which atoms can be added. In contrast, LBL and dendritic growth require higher supersaturation to form nuclei. A number of materials, including oxides, hydroxides, sulfides, and nitrides, can be grown into nanowire/tube morphologies through the SDD mechanism.[1–3,5,6] For example, Jin and co-workers demonstrated the solution growth of zinc oxide nanotubes by controlling the supersaturation.[1] In their study, the agreement between the experimental growth kinetics and those predicted from crystal-growth theories confirms that the growth of these nanotubes is driven by dislocations. The extension of SDD growth to nanoplate morphology has been realized in a few cases, for example, for the synthesis of zinc hydroxy sulfate and Au nanoplates.[7,8] However, SDD growth has not been observed for two-dimensional (2D) layered materials, which are in an entirely different category and have been attracting increasing attention, such as bismuth selenide (Bi_2Se_3).

Bi_2Se_3 is historically known for its thermoelectric properties and was recently confirmed to be a promising topological insulator material.[9,10] To date, Bi_2Se_3 nanoribbons and nanoplates have been synthesized by solution and vapor methods.[11–13] Bi_2Se_3 consists of planar quintuple layers (QLs, ca. 1 nm thick), which are five covalently bonded atomic sheets in the order Se–Bi–Se–Bi–Se (Figure 1 A). The QLs are stacked along the *c* axis and weakly bonded by van der Waals interactions.[14] The incorporation of screw dislocation into rhombohedral Bi_2Se_3 can presumably transform the layered structure into a continuous spiral belt (Figure 1 B) and thus create a drastically different type of platelike Bi_2Se_3 material.

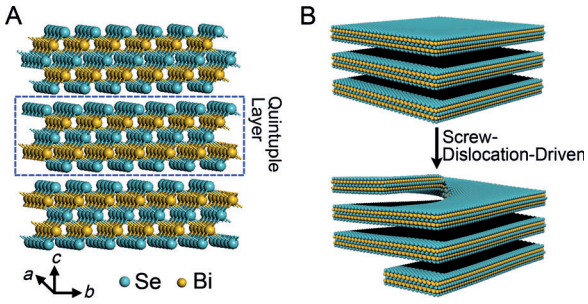

Figure 1. A) The layered rhombohedral crystal structure of Bi_2Se_3. B) Schematic representation of the incorporation of screw dislocation into the layered structure of Bi_2Se_3.

[*] A. Zhuang, J.-J. Li, Y.-C. Wang, X. Wen, Y. Lin, Prof. X. Wang, Prof. J. Zeng
Hefei National Laboratory for Physical Sciences at the Microscale and Collaborative Innovation Center of Suzhou Nano Science and Technology, University of Science and Technology of China
Hefei, Anhui 230026 (P. R. China)
E-mail: zengj@ustc.edu.cn
Homepage: http://zengnano.ustc.edu.cn/

A. Zhuang, J.-J. Li, X. Wen, Prof. X. Wang
Department of Physics
University of Science and Technology of China
Hefei, Anhui 230026 (P. R. China)

Prof. B. Xiang, Prof. J. Zeng
Center of Advanced Nanocatalysis (CAN-USTC) and School of Chemistry and Materials Science
University of Science and Technology of China
Hefei, Anhui 230026 (P. R. China)

[**] This research was supported by MOST of China (2014CB932700 and 2011CB921403), the NSFC (Grant Nos. 21203173, 51371164, and J1030412), Strategic Priority Research Program B of the CAS (Grant No. XDB01020000), and Fundamental Research Funds for the Central Universities (WK2340000050 and WK2060190025).

Supporting information for this article is available on the WWW under http://dx.doi.org/10.1002/anie.201403530.

Herein, we demonstrate a first, controlled synthesis of spiral-type Bi_2Se_3 nanoplates with screw dislocations and describe their use as a good platform to deepen our understanding of SDD growth. The products showed two sets of centrosymmetric helical fringes on the top and bottom surfaces. These helical fringes directly support the existence of screw dislocation and indicate the bidirectional spiral growth process. Other types of evidence, including herringbone contours, spiral arms, and hollow cores, were distinguished to support the bipyramid-like structure and SDD growth mode. Through manipulation of some of the reaction parameters, including the precursor concentration, the pH value, and the amount of reductant, we could tune the supersaturation in the regime of SDD growth to LBL growth and thus obtain smooth (conventional) Bi_2Se_3 nanoplates and intermediate products. The SDD growth process was investigated on intermediate products with preliminarily developed spiral-growth steps.

In a standard synthesis, the reaction was carried out in ethylene glycol (EG; 10 mL) with poly(vinylpyrrolidone) (PVP; 11 mg), L-ascorbic acid (AA; 43.5 mg), and hydrochloric acid (HCl; 20 μL, 11.8 M) at 175 °C under a N_2 atmosphere. The reaction was started by the rapid injection of a solution of $Bi(NO_3)_3{\cdot}5H_2O$ (2.5 mg) and Na_2SeO_3 (1.3 mg) in EG (2.5 mL). Because HCl can effectively lower the reducing capacity of AA by changing the pH value of the mixture,[15] the reduction of SeO_3^{2-} ions to Se^{2-} ions was suppressed to guarantee a relatively low supersaturation level. After 2 h, the color of the solution had changed to dark gray, which indicated the formation of products. Figure 2A shows a SEM image of the as-synthesized nanocrystals. The majority of products were hexagonal and platelike, with a typical lateral size of 2–5 μm and a thickness of approximately 60 nm. Powder X-ray diffraction (PXRD, Figure 2B) confirmed that the products were rhombohedral Bi_2Se_3 (JCPDS No. 89-2008; $a = 4.139$ Å, $c = 28.636$ Å). Through detailed examination of the samples by SEM, we found that they all contained helical fringes on the surfaces. Figure 2C shows the SEM image of a representative individual nanoplate with a single-helical pattern and a helical core located at the center. The well-defined layered structure of Bi_2Se_3 made it easy to accurately define the elementary Burgers vector of the screw dislocations as 1 QL. Atomic force microscopy (AFM) measurements (Figure 2D,E) clearly show a dislocation hillock, in which the terrace width (λ) is approximately 65 nm and the step height (h) is approximately 1 nm (Figure 2F), that is, 1 QL, equal to the elementary Burgers vector. Other types of products characterized by a single dislocation with multiple elementary Burgers vectors or by multiple dislocations with multiple elementary Burgers vectors were also observed (see Figure S1 in the Supporting Information for SEM images). We refer herein to all products as spiral-type Bi_2Se_3 nanoplates.

Since Bi_2Se_3 is more stable against a high-energy electron beam than, say, hydroxides,[7] we were able to undertake meticulous microscopic analysis and obtain state-of-the-art images of nanoplates with screw dislocations. Figure 3A shows a high-angle annular dark-field scanning TEM (HAADF-STEM) image of a representative spiral-type

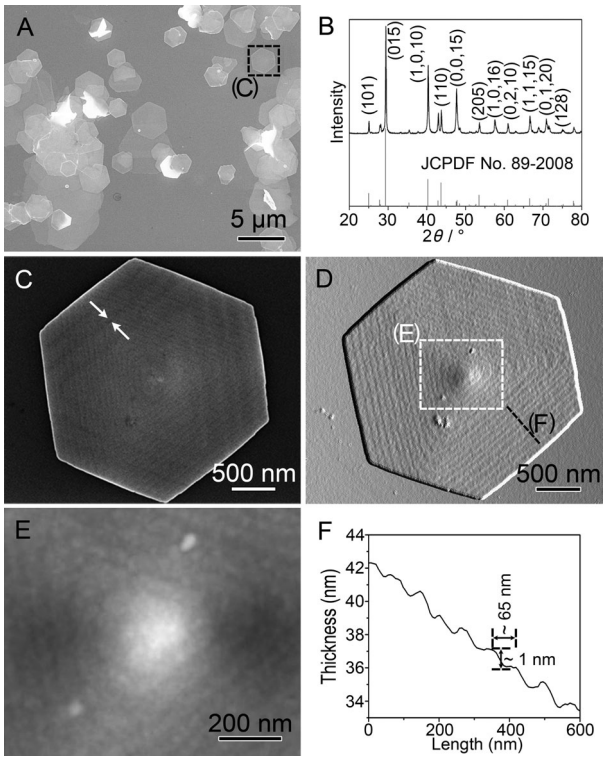

Figure 2. A) Low-magnification SEM image of Bi_2Se_3 nanoplates obtained from a standard synthetic procedure. B) PXRD pattern of the products in comparison with the reference Bi_2Se_3 diffractogram. C) High-magnification SEM image of a representative individual spiral-type Bi_2Se_3 nanoplate. The white arrows mark a set of reverse sparse trigonal fringes. D) AFM amplitude image of the nanoplate. E) Higher-magnification AFM amplitude image of the region marked by a white square in (D). F) AFM height profile of the nanoplate along the dashed black line in (D).

nanoplate. There are two sets of densely distributed centrosymmetric helical fringes, as marked by black and white dotted triangles. The magnified image of the central region shows the helical fringes more clearly (Figure 3B). The corresponding SEM and AFM images, however, show only one set of helical fringes on the top surface (see Figure S2). One can infer from these observations that the spiral growth mode of Bi_2Se_3 was bidirectional. The bidirectional growth is expected, since when there is no substrate, the dislocation has to end on two surfaces, and the growth is allowed in both directions theoretically.[8] A high-resolution TEM (HRTEM) image (Figure 3C) of the region marked by the white box in Figure 3A gives a direct view of hexagonal lattice fringes with a lattice spacing of 2.1 Å, which corresponds to $(11\bar{2}0)$ planes. The corresponding selected-area electron diffraction (SAED) pattern (Figure 3D) proves the high quality of single crystallinity and indicates that Bi_2Se_3 grew laterally along the $[11\bar{2}0]$ direction and vertically along the [0001] direction, with $(01\bar{1}0)$ facets on the sides. Energy-dispersive X-ray (EDX) spectroscopy was carried out to reveal the chemical composition. It was evident that the nanoplate was composed of Bi and Se with an atomic ratio of 2:3 (see Figure S3A) and that the two elements were uniformly distributed (see Figure S3B). Bright-field TEM images (Figure 3E; see also Figure S4)

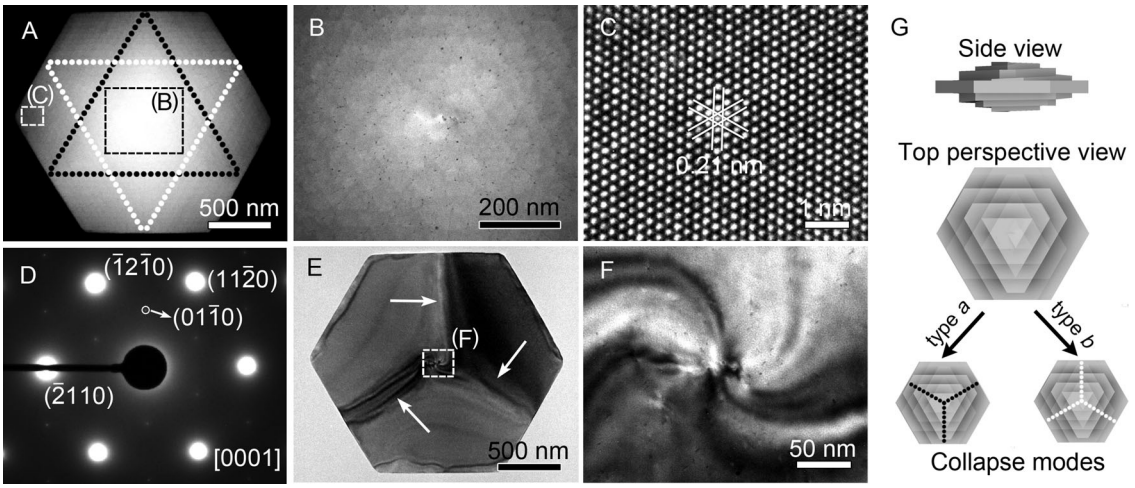

Figure 3. A) HAADF-STEM image of a spiral-type Bi_2Se_3 nanoplate. The centrosymmetric helical fringes are marked by black and white dotted triangles. B) Magnified HAADF-STEM image of the region marked by a black box in (A). C) HRTEM image of the region marked by a white box in (A). D) Corresponding SAED pattern along the Bi_2Se_3 [0001] direction. E) Bright-field TEM image of the nanoplate showing the herringbone contours, which are labeled with white arrows. F) Magnified TEM image of the white box in (E), showing spiral arms at the center of the nanoplate. G) Side and top perspective views of a typical spiral-type nanoplate, illustrating the two types of collapse modes. The black and white dotted tripod lines indicate different orientations of herringbone contours.

revealed that most of the nanoplates had contrast herringbone contours (labeled with white arrows in Figure 3E). Unlike in the HAADF-STEM images, the helical fringes can hardly be seen. At the center, where the helical core is located, however, spiral arms were found (Figure 3F).

On the basis of these observations, a scheme was drawn to model the examined nanoplate. As shown in Figure 3G, bidirectional growth steps of the nanoplate lead to the formation of a bipyramid-like structure, and the nanoplate shows helical fringes in the top perspective view. A nanoplate lying on a flat TEM grid is supported on only a tiny contact area around the center (or the dislocation core). Hence, the other edge area will tend to drop downward (or collapse) owing to gravity, thus generating tension in the nanoplate. As a consequence, herringbone contours will form. The two possible collapse modes are differentiated by the fracture lines, which are parallel either to the helical fringes on the top surface (type *a*) or to those on the bottom surface (type *b*). The two types of herringbone contours, which take the shape of the ridge of dislocation hillocks, were both discovered (see Figure S5). Despite the clear difference in the two collapse modes, it is difficult to determine which is more likely to happen. The above analysis suggests that it is reasonable to assume that the reverse sparse trigonal fringes shown in Figure 2C (marked by two white arrows) also originate from edge collapse of the nanoplate.

To elucidate the mechanism of formation of the spiral arms, it is necessary to rule out the influence of the herringbone contour at the overlapped area. One approach to inhibit the evolvement of herringbone contours is to synthesize nanoplates with smaller slopes of the dislocation hillock (i.e. h/λ). According to Burton–Cabrera–Frank (BCF) theory, the lateral step velocity (v_s), the growth rate normal to the surface (R_m), and the slope ($p = h/\lambda = R_m/v_s$) depends on the degree of supersaturation (σ) as follows: $v_s \propto \exp(\sigma)-1$, $R_m \propto [\exp(\sigma)-1]\sigma$, and $p \propto \sigma$.[16,17] Therefore, a lower value of σ should directly lead to nanoplates with smaller slopes. Spiral-type nanoplates with a lateral size of approximately 900 nm and a thickness of approximately 25 nm were obtained with decreased precursor concentrations of 1/4 of those used in the standard procedure (Figure 4A). The average value of λ was increased to 100 nm, and that of h was still maintained at 1 nm. As expected, all nanoplates (Figures 4B; see also Figure S6) showed no obvious herringbone contours; instead, over 70% of them displayed contrast spiral arms that initiated from the dislocation core. Since the collapse and thus the herringbone contours did not occur in this case, it is conceivable that the spiral arms are not a simple extension of herringbone contours to the dislocation core. Instead, the observation of spiral arms is consistent with an earlier kinematic simulation of the diffraction contrast of electron microscopy images.[18] It was described that screw dislocation perpendicular to a thin film will cause crystal displacement and twisting with an intensity proportional to the distance from the dislocation line, thus resulting in an oscillation contrast pattern observed by electron microscopes. The decreased thickness and extended terrace width make the helical fringes more clearly observed by HAADF-STEM (Figure 4C,F). All nanoplates, regardless of the magnitude of the Burgers vector, were found to have a hollow core near the center (Figure 4D,G). The corresponding TEM images showed that the cores were definitely transparent to the electron beam (Figure 4E,H). The hollow cores can be interpreted as a result of the relaxation of strain energy for dislocations with large Burgers vectors, as observed for nonlayered materials.[1,5,6]

Inspired by this phenomenon, we carefully rechecked the products acquired from our standard synthesis and also discovered hollow cores (see Figure S7). The hollow cores were sometimes difficult to recognize because the electron

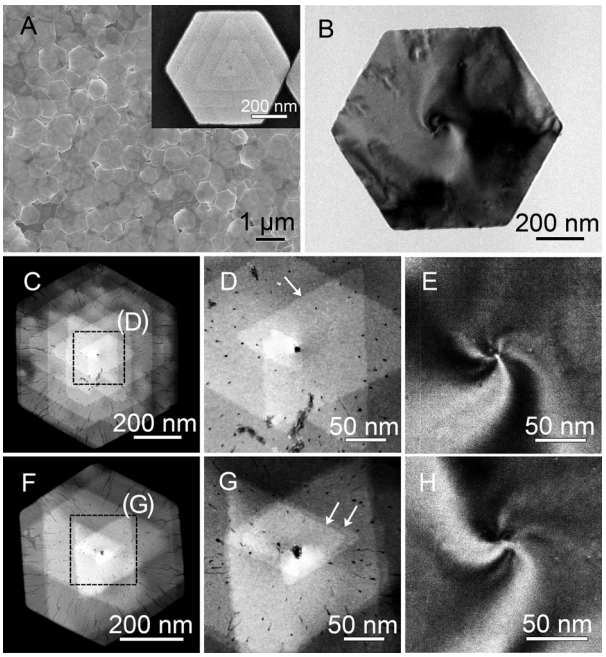

Figure 4. A) SEM image of spiral-type Bi_2Se_3 nanoplates synthesized at decreased precursor concentrations of 1/4 of the standard values. The inset is a high-magnification SEM image of an individual spiral-type nanoplate. B) TEM image of a nanoplate with spiral arm contours originating from the center. C) HAADF-STEM image of a nanoplate with a single elementary Burgers vector (indicated in (D) by a white arrow). D) Corresponding magnified HAADF-STEM image. E) High-magnification TEM image of the nanoplate center, showing an electron-transparent core. F–H) Parallel images with (C–E) of another nanoplate with two elementary Burgers vectors (indicated by two white arrows).

beam did not penetrate the leaning thicker vertical dimension. The average radius of the hollow core (r_0) was estimated for nanoplates with a single dislocation (see Figure S8). For nanoplates with one and two elementary Burgers vectors, r_0 was found to be 4.0 and 6.9 nm, respectively, thus indicating that larger Burgers vectors resulted in larger hollow cores to release more strain energy. However, the radius of the hollow core in Bi_2Se_3 nanoplates does not completely follow the relation $r_0 \propto B^2$ (specifically, $r_0 = B^2\mu/8\pi^2\gamma$, in which γ is the shear modulus and μ is the surface energy) that is applicable to isotropic materials, such as Au.[8,19] The reason for this deviation might be the existence of interlayer slips, which are caused by the weak bonding between QLs and provide an additional mode for the release of strain.

Considering that tuning of the supersaturation to a higher level could possibly lead to other growth modes, for example, LBL growth, we increased the concentration of the precursors. When the concentration of the precursors was increased by a factor of 1.5 with respect to the standard synthesis, a mixture of nanoplates with preliminarily developed dislocations and smooth nanoplates was obtained (see Figure S9A). The products were generally more transparent under an electron beam than that shown in Figure 3E, thus suggesting their thinner nature. The nanoplates with preliminarily developed dislocations are intermediate products of both SDD growth along the vertical dimension and LBL expansion along the lateral dimension. The small vertical size of Bi_2Se_3 nanoplates with preliminarily developed dislocations is due to the anisotropic layered structure of Bi_2Se_3. In general, atomic addition to the lateral dimension of Bi_2Se_3 nanocrystals is more thermodynamically favored than that to the vertical-thickness dimension;[11–13] the growth anisotropy can even reach several thousand as a result.[11] Therefore, LBL growth along the vertical dimension can be restricted to ensure the penetration of an electron beam with accessible energy. A further increase in the precursor concentrations to twice the standard values caused a marked change in morphology. All products were smooth on the top and bottom surfaces without helical fringes (see Figure S9B), thus indicating that the growth of nanoplates was dominated by lateral LBL expansion. Although it is clear that an increase in the concentration of precursors promotes higher supersaturation, an increase in the pH value owing to the presence of less HCl or an increase in the amount of AA had a similar effect by increasing the reducing power (see Figure S10).

By taking advantage of intermediate products on which dislocation had been preliminarily developed, we attempted to survey the SDD growth process. Figure 5A shows a TEM image of a typical intermediate nanoplate obtained with precursor concentrations 1.5 times those used in the standard synthesis. The bidirectional growth process can be deduced with ease; the trajectories of the two sets of centrosymmetric fringes are labeled with blue and red arrows, respectively. The slip plane of the nanoplate, that is, the $(01\bar{1}0)$ face, occurs along the diagonal lines of the hexagon-like structure. This observation is probably due to the higher growth rate along the $[\bar{2}110]$ direction and thus the higher probability of the development of slip planes. To confirm this hypothesis, we also examined individual nanoplates with multiple preliminarily developed screw dislocations (see Figure S11). The

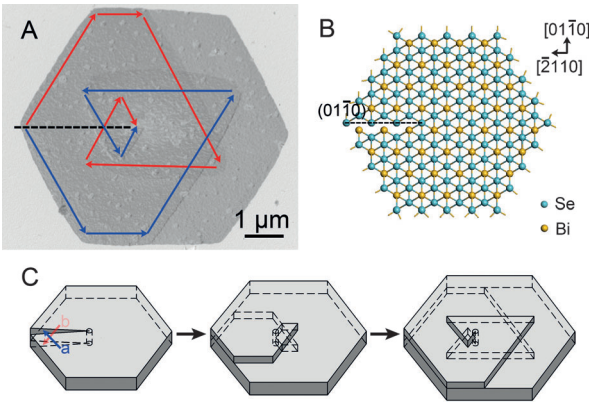

Figure 5. A) TEM image of a spiral-type nanoplate on which screw-dislocation growth has been preliminarily developed. The growth trajectories of the two sets of helical fringes are differentiated by red and blue. B) Ball-and-stick models of Bi_2Se_3 projected along the [0001] direction, illustrating that a slip appears on the $(01\bar{1}0)$ plane. C) Schematic diagrams showing the bidirectional helical growth process of a nanoplate. The blue (a) and red (b) arrows illustrate the growth steps on the top and bottom surfaces, respectively.

dislocations were randomly distributed over the corner sites, and for each dislocation, the corresponding slip plane took the same orientation as that shown in Figure 5A. As illustrated in Figure 5C, when a slip plane is generated, two growth steps (a and b) at the top and bottom faces are created and then move forward simultaneously. Since the angular growth velocity of the points on the surface step decreases with the distance from the dislocation core, it drops along the radial direction, thus leading to the development of helical fringes.[16] The dislocation core did not reside at the center of the nanoplate because of a shift in the growth mode, from dominant LBL growth to SDD growth, as the precursors were consumed with time.

In summary, we have reported the SDD growth of spiral-type Bi_2Se_3 nanoplates by a polyol synthesis. Screw dislocations on the nanoplates were substantiated by two sets of centrosymmetric helical fringes. The growth was found to evolve along the vertical dimension in a bidirectional manner. Through TEM analysis, we identified herringbone contours induced by collapse and spiral arms related to the dislocation core. By lowering the concentration of precursors and thus the supersaturation value, we were able to obtain spiral-type nanoplates with smaller slopes. These products do not show obvious herringbone contours and instead are often characterized by clearer helical fringes and spiral arms located around the dislocation core. Furthermore, hollow cores generated as a result of the relaxation of strain energy through dislocations were identified. By increasing the concentration of precursors, increasing the pH value, or adding more AA, we obtained nanoplates with preliminarily developed dislocations and smooth nanoplates dominated by LBL growth. The SDD growth process was distinguished on intermediate nanoplates with preliminarily developed dislocations. In general, the slip plane occurs along a diagonal line of the hexagon-like plate, and then two growth steps move forward on the top and bottom surfaces. We hope that understanding of the SDD bidirectional growth process of Bi_2Se_3 nanoplates can be extended to other 2D layered materials and will promote their design and practical application.

Received: March 20, 2014
Published online: May 14, 2014

Keywords: bismuth selenide · layered compounds · nanoplates · screw dislocation · supersaturation

[1] S. A. Morin, M. J. Bierman, J. Tong, S. Jin, *Science* **2010**, *328*, 476.
[2] a) M. J. Bierman, Y. K. A. Lau, A. V. Kvit, A. L. Schmitt, S. Jin, *Science* **2008**, *320*, 1060; b) J. Zhu, H. Peng, A. F. Marshall, D. M. Barnett, W. D. Nix, Y. Cui, *Nat. Nanotechnol.* **2008**, *3*, 477; c) F. Meng, S. Jin, *Nano Lett.* **2012**, *12*, 234.
[3] a) Y. K. A. Lau, D. J. Chernak, M. J. Bierman, S. Jin, *J. Am. Chem. Soc.* **2009**, *131*, 16461; b) H. Wu, F. Meng, L. Li, S. Jin, G. Zheng, *ACS Nano* **2012**, *6*, 4461; c) F. Meng, S. A. Morin, A. Forticaux, S. Jin, *Acc. Chem. Res.* **2013**, *46*, 1616.
[4] I. V. Markov, *Crystal Growth For Beginners: Fundamentals of Nucleation, Crystal Growth, and Epitaxy*, 1st ed., World Scientific Publishing, Singapore, **1995**.
[5] a) S. Iijima, *Nature* **1991**, *354*, 56; b) S. Jin, M. J. Bierman, S. A. Morin, *J. Phys. Chem. Lett.* **2010**, *1*, 1472; c) S. A. Morin, S. Jin, *Nano Lett.* **2010**, *10*, 3459; d) F. Meng, S. A. Morin, S. Jin, *J. Am. Chem. Soc.* **2011**, *133*, 8408; e) S. Hacialioglu, F. Meng, S. Jin, *Chem. Commun.* **2012**, *48*, 1174.
[6] a) B. W. Jacobs, M. A. Crimp, K. McElroy, V. M. Ayres, *Nano Lett.* **2008**, *8*, 4353; b) F. Ding, A. R. Harutyunyan, B. I. Yakobson, *Proc. Natl. Acad. Sci. USA* **2009**, *106*, 2506; c) D. Maestre, D. Haeussler, A. Cremades, W. Jaeger, J. Piqueras, *Cryst. Growth Des.* **2011**, *11*, 1117; d) D. Maestre, D. Haussler, A. Cremades, W. Jager, J. Piqueras, *J. Phys. Chem. C* **2011**, *115*, 18083; e) R. Rao, D. Liptak, T. Cherukuri, B. I. Yakobson, B. Maruyama, *Nat. Mater.* **2012**, *11*, 213.
[7] S. A. Morin, A. Forticaux, M. J. Bierman, S. Jin, *Nano Lett.* **2011**, *11*, 4449.
[8] a) E. Suito, N. Uyeda, *J. Electron Microsc.* **1960**, *8*, 25; b) E. Suito, N. Uyeda, *Bull. Inst. Chem. Res. Kyoto Univ.* **1965**, *42*, 511.
[9] a) Y. Sun, H. Cheng, S. Gao, Q. Liu, Z. Sun, C. Xiao, C. Wu, S. Wei, Y. Xie, *J. Am. Chem. Soc.* **2012**, *134*, 20294; b) Y. Min, J. W. Roh, H. Yang, M. Park, S. I. Kim, S. Hwang, S. M. Lee, K. H. Lee, U. Jeong, *Adv. Mater.* **2013**, *25*, 1425.
[10] a) H. Zhang, C.-X. Liu, X.-L. Qi, X. Dai, Z. Fang, S.-C. Zhang, *Nat. Phys.* **2009**, *5*, 438; b) Y. Xia, D. Qian, D. Hsieh, L. Wray, A. Pal, H. Lin, A. Bansil, D. Grauer, Y. S. Hor, R. J. Cava, M. Z. Hasan, *Nat. Phys.* **2009**, *5*, 398; c) J. E. Moore, *Nature* **2010**, *464*, 194; d) M. Z. Hasan, C. L. Kane, *Rev. Mod. Phys.* **2010**, *82*, 3045; e) X.-L. Qi, S.-C. Zhang, *Rev. Mod. Phys.* **2011**, *83*, 1057.
[11] D. S. Kong, W. H. Dang, J. J. Cha, H. Li, S. Meister, H. L. Peng, Z. F. Liu, Y. Cui, *Nano Lett.* **2010**, *10*, 2245.
[12] a) H. L. Peng, K. Lai, D. S. Kong, S. Meister, Y. Chen, X.-L. Qi, S.-C. Zhang, Z.-X. Shen, Y. Cui, *Nat. Mater.* **2010**, *9*, 225; b) D. S. Kong, J. C. Randel, H. L. Peng, J. J. Cha, S. Meister, K. Lai, Y. Chen, Z.-X. Shen, H. C. Manoharan, Y. Cui, *Nano Lett.* **2010**, *10*, 329; c) J. Zhang, Z. Peng, A. Soni, Y. Zhao, Y. Xiong, B. Peng, J. Wang, M. S. Dresselhaus, Q. Xiong, *Nano Lett.* **2011**, *11*, 2407; d) Y. Min, G. D. Moon, B. S. Kim, B. Lim, J.-S. Kim, C. Y. Kang, U. Jeong, *J. Am. Chem. Soc.* **2012**, *134*, 2872; e) D. S. Kong, K. J. Koski, J. J. Cha, S. S. Hong, Y. Cui, *Nano Lett.* **2013**, *13*, 632.
[13] a) L. D. Alegria, M. D. Schroer, A. Chatterjee, G. R. Poirier, M. Pretko, S. K. Patel, J. R. Petta, *Nano Lett.* **2012**, *12*, 4711; b) H. L. Peng, W. Dang, J. Cao, Y. Chen, D. Wu, W. Zheng, H. Li, Z.-X. Shen, Z. F. Liu, *Nat. Chem.* **2012**, *4*, 281; c) H. Li, J. Cao, W. Zheng, Y. Chen, D. Wu, W. Dang, K. Wang, H. L. Peng, Z. F. Liu, *J. Am. Chem. Soc.* **2012**, *134*, 6132; d) Y. Guo, M. Aisijiang, K. Zhang, W. Jiang, Y. Chen, W. Zheng, Z. Song, J. Cao, Z. F. Liu, H. L. Peng, *Adv. Mater.* **2013**, *25*, 5959.
[14] R. W. G. Wyckoff, *Crystal Structures*, Krieger, Malabar, FL, **1986**.
[15] J. Zhou, J. Zeng, J. Grant, H. Wu, Y. Xia, *Small* **2011**, *7*, 3308.
[16] W. K. Burton, N. Cabrera, C. Frank, *Philos. Trans. R. Soc. London Ser. A* **1951**, *243*, 299.
[17] H. H. Teng, P. M. Dove, J. J. De Yoreo, *Geochim. Cosmochim. Acta* **2000**, *64*, 2255.
[18] A. Howie, M. J. Whelan, *Proc. R. Soc. London Ser. A* **1962**, *267*, 206.
[19] F. C. Frank, *Acta Crystallogr.* **1951**, *4*, 497.

